PCCP

Accepted Manuscript

ROYAL SOCIETY OF CHEMISTRY

www.rsc.org/pccp

Mechanistic Details of Energy Transfer and Soft Landing in ala_2-H^+ Collisions with a F-SAM Surface

S. Pratihar, N. Kim, S. C. Kohale, and W. L. Hase*

Department of Chemistry and Biochemistry

Texas Tech University

Lubbock, Texas 79409-1061

*To whom correspondence should be addressed: bill.hase@ttu.edu

Abstract

Previous chemical dynamics simulations (*Phys. Chem. Chem. Phys.*, 2014, **16**, 23769-23778) were analyzed to delineate atomistic details for collision of N-protonated dialanine (ala_2-H^+) with a C_8 perfluorinated self-assembled monolayer (F-SAM) surface. Initial collision energies E_i of 5-70 eV and incident angles θ_i of 0° and 45°, with the surface normal, were considered. Four trajectory types were identified: (1) direct scattering; (2) temporary sticking/physisorption on top of the surface; (3) temporary penetration of the surface with additional physisorption on the surface; and (4) trapping on/in the surface, by physisorption or surface penetration, when the trajectory is terminated. Direct scattering increases from 12 to 100% as E_i is increased from 5 to 70 eV. For the direct scattering at 70 eV, at least one ala_2-H^+ heavy atom penetrated the surface for all of the trajectories. For ~ 33% of the trajectories all eleven of the ala_2-H^+ heavy atoms penetrated the F-SAM at the time of deepest penetration. The importance of trapping decreased with increase in E_i, decreasing from 84 to 0% with E_i increase from 5 to 70 eV at $\theta_i = 0^o$. Somewhat surprisingly, the collisional energy transfers to the F-SAM surface and ala_2-H^+ are overall insensitive to the trajectory type. The energy transfer to ala_2-H^+ is primarily to vibration, with the transfer to rotation ~ 10% or less. Adsorption and then trapping of ala_2-H^+ is primarily a multi-step process, and the following five trapping mechanisms were identified: (i) physisorption-penetration-physisorption (phys-pen-phys); (ii) penetration-physisorption-penetration (pen-phys-pen); (iii) penetration-physisorption (pen-phys); (iv) physisorption-penetration (phys-pen); and (v) only physisorption (phys). For E_i = 5 eV, the pen-phys-pen, pen-phys, phys-pen, and phys trapping mechanisms have similar probabilities. For 13.5 eV, the phys-pen mechanism, important at 5 eV, is unimportant. The radius of gyration of ala_2-H^+ was calculated once it is trapped on/in the F-SAM surface and trapping decreases the ion's compactness, in part by breaking hydrogen bonds. The ala_2-H^+ + F-SAM simulations are compared with the penetration and trapping dynamics found in previous simulations of projectile + organic surface collisions.

I. Introduction

Self-assembled monolayers (SAMs) on metal surfaces are widely used in nanoscience and nanotechnology.[1] Experimental[2-27] and computational simulation studies[28-41] have probed the dynamics of energy transfer,[2,3,16,18-22,26-41] surface adsorption,[18,22,28-30,34-36,41] and thermal accommodation[4-6,12,22-25] in collisions of gaseous projectiles with SAM surfaces. Amongst this work, studies of collisions of biological ions with SAM surfaces have a number of important technological applications.[12-15,23-25,42]

For the last two decades, peptide/protein collisions with organic surfaces has been a principal research interest of mass-spectrometry. Several chemical and physical processes may occur when a protonated peptide ion (peptide-H^+) collides with an organic surface.[43,44] They include surface-induced dissociation (SID),[2,3] soft-landing (SL),[4-6] and reactive-landing (RL).[7,8] In SID the projectile, energized by its collision with the surface, either dissociates upon impact with the surface (shattering)[2,45] or is scattered into the gas phase and then dissociates. SID is an important experimental tool for determining structural properties of ions,[9] and energetic and mechanistic information concerning their dissociation pathways.[10.11] For low collision energies the ion may adsorb on the surface intact, with or without charge retention, a process referred to as SL.[12] In RL the projectile forms chemical bonds with and chemisorbs on the surface.[13] SL and RL have numerous uses, [12-15,23-25,42] including preparation of protein or peptide arrays, development of novel biosensors and substrates for improved cell adhesion, purification of compounds from complex mixtures, and deposition of mass-selected cluster ions.[14,15]

Classical chemical dynamics simulations, based on accurate potentials, have proven to be an important tool to understand the atomistic details of projectile-surface collisions.[28-41,45] Energy transfer probabilities to the surface and projectile may be determined,[28-41,45] as well as features of the collision such as the importance of surface penetration[29,33-36,41,46,47] or physisorption.[34-36,41] Simulations of protonated peptide collisions with surfaces have been particularly useful in providing atomistic information regarding the energy transfer and shattering mechanisms for SID[38,39,45] and the dynamics for SL[41] and RL.[48]

Using an accurate gas-surface intermolecular potential fit to *ab initio* calculations,[49] energy transfer and SL were studied in a previous simulation of N-protonated dialanine (ala_2-H^+) collisions with a perfluorinated $CF_3(CF_2)_7S$- self-assembled monolayer (F-SAM) surface.[41] Excellent agreement was found between the experiment[27] and simulation percentages of the

collision energy transferred to the ala_2-H^+ internal degrees of freedom, and the shape of the distribution function for this energy transfer. In the work presented here the results of this previous simulation are further analyzed. The following four trajectory types, regarding the ala_2-H^+ dynamics, were identified in the simulations:[41] (1) direct scattering; (2) temporary sticking/physisorption on top of the surface; (3) temporary penetration of the surface, with and without additional sticking/physisorption on the surface; and (4) trapping on/in the surface, by physisorption or surface penetration, when the trajectory is terminated. The percentages of the trajectories which are of these types are now determined for each ala_2-H^+ + F-SAM incident collision energy and angle. Average percentage energy transfers, and their distributions, are also determined for each of the above four trajectory types. In addition, analyses are made of physisorption and surface penetration mechanistic pathways for ala_2-H^+ + F-SAM soft-landing. Comparisons are made with simulations of other projectile-surface collisions; i.e. penetration of surfaces by Ne,[29] $O(^3P)$,[34] and Xe[47] atoms and CO_2.[35]

II. Computational procedure

The methodology for the chemical dynamics simulations reported here was described in detail previously[41] and only a brief description is given here. The simulations were performed with the VENUS chemical dynamics computer program.[50,51]

A. Analytic potential energy function and parameters

The general analytic potential energy function used for the ala_2-H^+/F-SAM system is given by

$$V = V_{peptide} + V_{surface} + V_{surface,peptide} \quad (1)$$

where $V_{peptide}$ is the ala_2-H^+ intramolecular potential, $V_{surface}$ is the F-SAM surface potential, and $V_{peptide,surface}$ is the ala_2-H^+/F-SAM intermolecular potential. The AMBER molecular mechanics (MM) potential[52] was used for $V_{peptide}$. A local energy minimization procedure, using the VENUS computer program, was carried out to find the minimum energy conformer for ala_2-H^+, the same conformer as found in previous work.[40] The intramolecular potential includes harmonic stretches and bends, torsions treated as dihedral angles, and non-bonded Lennard-Jones interactions.

The explicit-atom (EA) model developed by Borodin and coworkers from electronic structure calculations[53] was used to represent the $CF_3(CF_2)_7S$- F-SAM monolayer. A large rigid border F-SAM model was chosen to account for lateral movement of each $CF_3(CF_2)_7S$- chain of the surface. It had 46 rigid exterior $CF_3(CH_2)_7S$ chains, 75 interior $CF_3(CF_2)_7S$ chains, both adsorbed on a single layer of 484 Au atoms held fixed at their equilibrium positions. This rigid border model gives statistically the same results as one with periodic boundary conditions (PBC).[40,41] Non-bonded Buckingham interactions were included between atoms of the $-CF_2-$, and $-CF_3$ groups and the atoms of the Au surface.[53]

Interactions between ala_2-H^+ and the F-SAM were expressed as a sum of two-body terms between the atoms of ala_2-H^+ and the C and F atoms of the F-SAM. In this explicit atom model, the intermolecular potential is a sum of atom-atom pair interactions and is given by

$$V_{surface,peptide} = \sum_i \sum_j \left\{ A_{ij} e^{-B_{ij} r_{ij}} + \frac{C_{ij}}{r_{ij}^{n_{ij}}} + \frac{D_{ij}}{r_{ij}^{m_{ij}}} \right\} \quad (2)$$

where i and j refer to atoms belonging to ala_2-H^+ and the F-SAM, and r_{ij} is their interatomic distance. This potential has quite accurate short-range repulsive and long-range attractive interactions. The parameters for the two-body potentials were determined by fits to intermolecular potential energy curves obtained by MP2/aug-cc-pVTZ *ab initio* calculations.[49]

Interaction potentials were not included between ala_2-H^+ and the surface gold atoms. The ala_2-H^+ cations do not penetrate deep enough for these interactions to be important. As discussed below, in Section III.A, the deepest penetration is for the simulations with a collision energy of 70 eV, for which an ala_2-H^+ heavy atom penetrates as deep as CF_3-CF_2-CF_2-CF_2-CF_2- of the F-SAM. There remains a substantial separation, $-CF_2$-CF_2-CF_2-S-Au(s) with the surface.

B. Trajectory simulation

Trajectory initial conditions were chosen to mimic the experimental conditions.[27] The center of a beam of ala_2-H^+ projectiles with fixed initial translational energy (E_i) and angle of incidence (θ_i) was aimed at the center unit cell of the F-SAM surface. The radius of the beam was chosen to overlap the unit cell of the surface. The peptide projectile for each trajectory was randomly placed in the cross section of this beam and randomly rotated about its center of mass to ensure random orientation of the peptide ion with respect to the surface.[28]

Initial conditions for the $CF_3(CF_2)_7S$- SAM were chosen by assigning velocities to its atoms, sampled from their Maxwell-Boltzmann distributions at 300K. The surface was then equilibrated for 8 ps, with velocity rescaling for an initial 6 ps, followed by 2 ps of a molecular dynamics equilibration without velocity rescaling. The average temperature of the surface after equilibration was 300 ± 5 K. For the equilibrated SAM, the average distance in the perpendicular z-direction between the S-atom and the F atoms of the terminal $–CF_3$ groups is 9.3 Å. The C-C bond lengths are 1.56 Å. The backbones of the $CF_3(CF_2)_7S$ are tilted by ~12° with respect to the Au surface normal and the alkyl chains have helical conformations. These structural attributes are in good agreement with experiment.[54]

The C-C bond lengths are 1.56 Å and the alkyl chains have helical conformations. The structure of the equilibrated F-SAM is in good agreement with experiment.[54] Experiment shows that the F-SAM forms a hexagonal close-packed structure with the nearest neighbor direction rotated ~ 30° with respect to the Au{111} lattice and the backbone of the CF_3-$(CF_2)_7$-S moiety has a small tilt angle of 12 ± 2° with respect to the surface normal. The model used for the F-SAM gives 30.0^o and 13.7^o for these two angles.[35] The experimental average distance between the terminal C-atoms is 5.78 ± 0.001 Å and the F-SAM model's value is 5.89 ± 0.01 Å.[40]

Initial conditions for the peptide's vibrational modes were chosen via the quasiclassical normal mode method,[55,56] which includes zero point energies. The energy for each normal mode was selected from the mode's 300 K harmonic oscillator Boltzmann distribution. Energy was randomly partitioned between kinetic and potential by choosing a random phase for each normal mode. A 300 K rotational energy of *RT/2* was added to each principal axis of rotation of the peptide ion. Details for this sampling of vibrational and rotational energies have been given previously.[57]

The nature of the classical intramolecular motion of a molecule is affected by its total energy.[58] If ala_2-H^+ was excited classically, without zero point energy, its total energy content would be much lower and its motion more regular than for the quasiclassical sampling performed here of the quantum energy levels. Previous studies have shown that quasiclassical sampling with zero point energy is necessary to obtain accurate short time energy transfer dynamics.[59,60] However, in future work it would be of interest to study peptide-H^+ + surface energy transfer with a peptide-H^+ classical Boltzmann internal energy distribution instead of the quasiclassical quantum Boltzmann distribution used here. It is noteworthy that quasiclassical quantum

sampling and classical molecular dynamics sampling of the vibrational energy levels of a H-SAM surface at 300 K give very similar collisional energy transfer efficiencies.

Ensembles of 400 trajectories were simulated for each set of initial conditions of fixed E_i and θ_i. The time step was 0.02 ps for trajectory integration using an Adams-Moulton algorithm,[61-63] a standard option in VENUS.[50,51]

III. Results and discussion

As discussed in the Introduction, there are the following four trajectory types and their percentages were determined for each E_i and θ_i simulation: i.e., (1) direct scattering; (2) temporary sticking/physisorption on top of the surface; (3) temporary penetration of the surface with additional physisorption on the surface; and (4) trapping on/in the surface, by physisorption or surface penetration, when the trajectory is terminated. Average percentage energy transfers, and their distributions, are determined for each of these four trajectory types. Analyses are also made of physisorption and surface penetration mechanistic pathways for ala_2-H^+ + F-SAM soft-landing.

For trajectories that scatter off the surface, the collision translation energy E_i is partitioned between the final translational energy E_f, the internal energy of the ion, $\Delta E_{int,}$ and surface vibrations ΔE_{surf} following the relation

$$E_i = E_f + \Delta E_{int} + \Delta E_{surf} \tag{3}$$

The internal energy of the ion is a summation of its vibration (vib) and rotation (rot) energies. Hence the change of internal energy follows the relation

$$\Delta E_{int} = \Delta E_{rot} + \Delta E_{vib} \tag{4}$$

Direct scattered trajectories are those with only one inner turning point (ITP) in their motion perpendicular to the surface plane. Physisorption is an event with more than one ITP, without penetration into the surface. Physisorption trajectories are adsorbed on the surface for a substantial period of time. For F-SAM penetration, at least one ala_2-H^+ heavy atom is inside the F-SAM, i.e. it is within the midpoint of the average 300 K perpendicular distances of the C-

atoms of the terminal $–CF_3$ and adjacent $–CF_2–$ groups above the Au-layer. The non H-atoms of ala_2-H^+ are the heavy atoms. Animations of different trajectory types are available on the web portal hase-group.ttu.edu.

A. Percentages of different trajectory types and their residence times

The percentage of the four different trajectory types, versus E_i and θ_i, are listed in Table 1. The different dynamics for the direct scattering, temporarily penetrated/physisorbed, and trapped trajectories are illustrated in Figure 1. Of interest is that, though the directly scattered trajectory penetrated the surface, it was not trapped in/on the surface. This is discussed in more detail below.

There are interesting trends in the percentages of the four different trajectory types versus E_i and θ_i. The following is found for the $\theta_i = 0^o$ simulations. The percentage of direct scattering increases from 12 to 100% with increase in E_i from 5 to 70 eV. For the direct scattering at 70 eV, at least one ala_2-H^+ heavy atom penetrates the surface for all of the trajectories. The percentage of trajectories, for which ala_2-H^+ is only temporarily physisorbed on the "top" of the F-SAM, is always small and decreases with increase of E_i. The percentage of trajectories which both penetrate and physisorb on the F-SAM first increases with increase in E_i, but becomes zero at 70 eV. This percentage is as large as 13% at E_i of 30 eV. The percentage of trajectories trapped in/on the F-SAM at the conclusion of the trajectories decreases with increase in E_i, becoming zero at E_i of 70 eV. Apparently, as E_i is increased it becomes more difficult for the F-SAM to accommodate the collision energy for trapping to occur.

Effects on the dynamics of changing θ_i from 0 to 45 degrees depend on the collision energy. For E_i = 5 eV the percentage of directly scattered trajectories is statistically the same for 0 or 45 degrees, but trapping at the conclusion of the trajectory is predominant for $\theta_i = 0^o$. The incident angle has a major effect on the trajectory types at E_i = 22.5 eV. With increase in θ_i to 45°, the percentage of directly scattered trajectories increases by a factor of ~2.0, while the percentage of trapped trajectories becomes quite small.

As E_i is increased the trajectories penetrate the F-SAM more deeply. As discussed below in Section III C, for the low E_i of 5 and 13.5 eV only penetration of the top of the F-SAM is important. However, for E_i of 30 and 70 eV ala_2-H^+ penetrates more deeply. A deep penetration 70 eV trajectory is depicted in Figure 2 and also in Figure 2 of reference 41. Figure 3 gives distributions of the deepest penetration of the F-SAM by an ala_2-H^+ heavy atom, for the E_i of 30

and 70 eV simulations with $\theta_i = 0^o$. There are seven C-C midpoints for the $CF_3(CF_2)_7S$- chain, with CF_3-CF_2 identified as midpoint 1, and the distributions give the deepest midpoint penetration for the trajectories in the ensemble. For the 30 and 70 eV simulations, the deepest penetration is midpoint 2 and 5, respectively. Thus, for the 70 eV simulation, there is penetration deeper than CF_3-CF_2-CF_2-CF_2-CF_2-. The average number of ala_2-H^+ heavy atoms inside the F-SAM is 8.8, at the deepest penetration for the 70 eV trajectories. For ~33% trajectories all of the 11 heavy atoms were inside the F-SAM surface at the time of deepest penetration. For both these 30 and 70 eV simulations, there are no ala_2-H^+ heavy atoms which reach the Au surface.

As done in previous work,[29,34,64] a distance criterion was used to determine a residence time for ala_2-H^+ interacting with the F-SAM. The interaction of ala_2-H^+ with the F-SAM was identified as beginning when a distance between any heavy atom of ala_2-H^+ and any F-atom of the terminal $–CF_3$ groups of the F-SAM became less than 4 Å, while the ending was determined when all the heavy atoms are more than 4 Å away from the surface after desorption. The difference between these two times is the residence time. The average residence time for a particular E_i and θ_i, and for a particular trajectory type, is identified as τ_{res}. Values for τ_{res} were determined for the directly scattered trajectories at $\theta_i = 0^o$ with E_i of 13.5 and 30 eV, and the respective values are 0.70 and 0.97 ps. For E_i of 70 eV and θ_i of 0°, all of the trajectories directly scatter from the surface with only one ITP. The average residence time is 0.7 ps for the 70 eV and 0° directly scattered trajectories.

As shown in Table 2, for the trajectories which temporarily only physisorb or both penetrate and physisorb, τ_{res} ranges from 1 to 4 ps, with the value decreasing with increase in E_i. The τ_{res} values are similar for these two types of temporarily trapped trajectories. In addition, τ_{res} is not strongly affected by θ_i.

B. Different trajectory types and their energy transfers

As discussed previously,[41] the distribution and average of the energy transferred to ala_2-H^+ internal degrees of freedom, for the ala_2-H^+ + F-SAM collisions, are in excellent agreement with experiment. Of interest is how the ala_2-H^+ + F-SAM energy transfers depend on the trajectory type, and in Table 3 the average energy transfer to ΔE_{int}, ΔE_{surf}, and E_f are given for each trajectory type of each E_i, θ_i simulation.

The most striking aspect of the results in Table 3 is the overall insensitivity of the average energy partitioning with respect to the trajectory type. Except for the simulation at 22.5 eV and

45°, there is more energy transferred to ala_2-H^+ internal degrees of freedom and less to the surface for directly scattered trajectories, as compared to those which are temporarily physisorbed or temporarily penetrate and physisorb, but the difference is rather small. There is a similar small difference in the ΔE_{int} transfer to ΔE_{vib} and ΔE_{rot} for these two trajectory types. For the direct scattering, the $<\Delta E_{vib}>$ percentage is somewhat smaller and that for $<E_{rot}>$ somewhat larger, than for the temporarily trapped trajectories.

For the direct scattering trajectories, which penetrate the surface, the transfer of energy to internal degrees of freedom of ala_2-H^+, ΔE_{int}, decreases as the residence time for the ala_2-H^+ + F-SAM interaction increases. This is illustrated by the scatter plot in Figure 4 for the E_i = 30 eV and $\theta_i = 0^o$ simulations. As the residence time increases for these directly scattered trajectories, energy transfer to ΔE_{int} decreases and that to ΔE_{surf} increases.

Distributions of energy transfer to ala_2-H^+ vibration and rotation, ΔE_{vib} and ΔE_{rot}, are given in Figures 5-7 for collisions at $\theta_i = 0^o$ and E_i = 13.5, 30 and 70 eV. For 13.5 and 30 eV, distributions are given for both directly scattered trajectories and those which temporarily physisorb with and without penetration. For 70 eV only the former occur. The distributions are quite broad, particularly for ΔE_{vib}. As shown in Table 3, the average percentage energy transfer to ΔE_{rot} is small. However, there are a small number of collisions for which ΔE_{rot} is large. For E_i = 13.5 eV, ΔE_{rot} is as large as 22.3 and 15.5 kcal/mol, respectively, for the directly scattered trajectories and those which temporarily physisorb with and without penetration. At E_i of 30 eV these ΔE_{rot} are 43.9 and 58.5 kcal/mol. For the directly scattered trajectories at E_i = 70 eV, the largest ΔE_{rot} is 43.3 kcal/mol.

C. Dynamics and mechanisms for physisorption and trapping

Adsorption of peptide ions on the F-SAM surface is a complex process. Interactions between the surface and peptide are long range, and their overall strength is substantially higher than the peptide's thermal translational energy. Furthermore, as a result of these peptide/surface interactions, adsorption of the peptide is expected to strongly influence the peptide's shape and size. The kinetics and thermodynamics of conformational changes of the peptide ion on/in the surface, during and after adsorption, are complex. As shown in Table 3, our simulations find that low energy collisions, with $\theta_i = 0^o$ normal incident angle collisions, are most effective for ala_2-H^+ trapping on/in the F-SAM surface.

Mechanisms for trapping of ala_2-H^+ on the F-SAM surface were investigated for E_i of 5 and 13.5 eV with $\theta_i = 0^o$. Due to the flexibility of the peptide ion, it was difficult to delineate the mechanistic details of the ion's adsorption and then trapping on the F-SAM at the conclusion of the 10 ps trajectories. From a detailed analysis of the trajectories, it was found that adsorption and then trapping of ala_2-H^+ is primarily a multi-step process. The following were identified as mechanisms for adsorption followed by trapping on the F-SAM: (i) physisorption-penetration-physisorption (phys-pen-phys); (ii) penetration-physisorption-penetration (pen-phys-pen); (iii) penetration-physisorption (pen-phys); (iv) physisorption-penetration (phys-pen); and (v) only physisorption (phys). The fraction of the trajectories that followed these mechanism are listed in Table 4. To clarify these mechanism identifiers, "physisorption-penetration-physisorption" means that ala_2-H^+ first physisorbs on the F-SAM, then penetrates the surface, and is then physisorbed when the trajectory is terminated. As described above, for penetration, at least one ala_2-H^+ heavy atom is within the midpoint of the average 300 K perpendicular distances of the C-atoms of the terminal $–CF_3$ and adjacent $–CF_2–$ groups above the Au-layer.

As shown in Table 1, for the 5 eV simulation in Table 4, 84% of the ala_2-H^+ ions are trapped in/on the F-SAM at the conclusion of the trajectories. Of this percentage, 40% first penetrate the F-SAM, while 44% first physisorb. Given the statistical uncertainties, the pen-phys-pen, pen-phys, phys-pen, and phys trapping mechanisms have similar probabilities. For the 13.5 eV simulation, 65% of the trajectories are trapped and the phys-pen mechanism, important at 5 eV, is unimportant at this higher energy. The dominant trapping mechanism is pen-phys, with 47% of the trajectories first penetrating and only 18% first physisorbing.

Analysis were performed, for each of the $\theta_i = 0^o$ and E_i of 5 and 13.5 eV trajectories, to determine the average fraction of the ala_2-H^+ eleven heavy atoms which penetrate the F-SAM (f_{pen}) for an event where ala_2-H^+ is trapped on/in the F-SAM at the conclusion of the trajectory. This was done, for each of these trajectories, by determining the number of heavy atoms which penetrate the F-SAM versus time, where this analysis versus time was initiated when ala_2-H^+ was 4 Å above the F-SAM as described in the above section III A. From this time-dependent information, the average number of heavy atoms that penetrated the F-SAM was determined for each trajectory, which was then combined for the ensemble of trajectories for a particular E_i, θ_i simulation.

Figure 8 presents, for the 5 eV and 13.5 eV simulations with θ_i = 0°, the resulting distribution of the average fraction, f_{pen}, of ala$_2$-H$^+$ heavy atoms which penetrate the F-SAM once ala$_2$-H$^+$ passes within the 4 Å surface separation as described in section III A. For both simulations the most probable f_{pen} is between 0.9 and 1.0, and average f_{pen} is 0.7. For these two E_i most of the penetration is near the top of the CF_3-CF_2-CF_2-CF_2-$(CF_2)_4$ fluorinated chains. The following are the respective percentages for penetration between the CF_3-CF_2 and the next CF_2-CF_2 midpoints, and between this latter midpoint and the next CF_2-CF_2 midpoint; i.e. between midpoints 1-2 and 2-3. They are 29 and 24 % and 33 and 23% for the 5 and 13.5 eV simulations, respectively.

To investigate conformational changes of ala$_2$-H$^+$ trapped on/in the F-SAM, the radius of gyration was calculated for these ions. The radius of gyration is given by

$$R_g = \sqrt{\frac{\sum_i m_i (r_i - r_{cm})^2}{\sum_i m_i}} \tag{5}$$

where m_i is the mass of atom i, r_i is the position of atom i, and r_{cm} is the position of the center of mass. R_g gives a rough measure of the compactness of a structure. The R_g at the 10 ps termination of the 5 and 13.5 eV simulations, with θ_i = 0°, were calculated and their distributions are shown in the bottom panel of Figure 9. For both distributions, R_g ranges from 2.1 to 2.8 Å with the most probable value between 2.4 and 2.6 Å. R_g for the ala$_2$-H$^+$ optimized structure is 2.35 Å. Structures of optimized ala$_2$-H$^+$ and the ion with R_g of 2.77 Å are compared in the top panel of Figure 9. The structure of the trapped ion becomes less compact by breaking a H---O hydrogen bond. Trapping of ala$_2$-H$^+$ on/in the F-SAM decreases its compactness.

IV. Penetration and trapping: Comparisons with previous studies

It is of interest to compare the results of the current ala$_2$-H$^+$ + F-SAM simulation, regarding surface penetration and trapping, with the findings of previous simulations of projectile + organic surface collisions. For the ala$_2$-H$^+$ + F-SAM collisions, surface penetration becomes more important as the collision energy is increased, but trapping on/in the surface becomes less

probable. The probabilities of both penetration and trapping decreases as the incident angle θ_i is increased from 0 to 45°, where θ_i of 0° is a perpendicular, normal collision.

Table 5 summarizes the results, regarding penetration and trapping, from previous simulations of projectile + organic surface collisions.[16,29,35,64-66] For the first entry in Table 5,[64] the dynamics are studied versus the C_{12} H-SAM inter chain spacing for Ar collisions, where the normal spacing is 4.98 Å. Decreasing the spacing decreases the percentage trapping, which becomes very small for the tightest spacing and "stiffest' surface. The percentage of the collision energy transferred to $<E_f>$ is substantially smaller for the least dense surface. In comparing Ne, Ar, and Kr collisions with the C_{15} H-SAM,[65] trapping is most important for Kr and the $<E_f>$ percent is largest for Ne. The penetration percentages for the three rare gases differ by less than a factor of two. For the C_{15} F-SAM as compared to the H-SAM,[65] penetration by Ar and Kr is strongly suppressed and the $<E_f>$ percent is much larger for Ne. The dynamics for Ne colliding with the C_6 H-SAM are consistent with those above for the C_{15} H-SAM.[29] For the C_6 H-SAM simulations, both E_i and θ_i were varied and penetration increased with decrease in θ_i and increase in E_i. The percentage transfer to $<E_f>$ decreased with increase in E_i, but was insensitive to θ_i. Additional simulations[67,68] of Ne + C_6 H-SAM collisions give results similar to those in Table 5.

As shown in Table 5, the dynamics of CO and OH collisions with H-SAM and F-SAM surfaces are not strongly dependent on their vibrational and rotational quantum numbers.[16,66] For these collisions, the H-SAM surface has much more trapping, with a very small amount of penetration. For the fluorinated surface there is no penetration and energy transfer to $<E_f>$ is larger. For CO_2 + C_8 F-SAM[35] the scattering is somewhat unusual in that penetration decreases with increase in E_i.

In the following, within this section, additional simulations of projectile + surface collisions are summarized, but not included in Table 5. For Ne + C_{12} H-SAM collisions, at a surface temperature of 135 K,[69] no penetration of the surface is observed in comparison to the results in Table 5 for 300 K. Apparently this arises from a much more rigid surface at the lower temperature, not allowing entry of the light Ne-atom within the surface. In contrast, for simulations of the more massive Xe-atom scattering with the 135 K C_{12} H-SAM surface, deep penetration of the H-SAM is observed.[18] However, the atoms do not remain trapped in the surface, but are expelled with an angular distribution peaked close to the direction of the alkyl chains for the H-SAM.

An extensive set of simulations were performed for Ar colliding with the C_8 F-SAM, for E_i of 6 to 12 eV and θ_i of 0° and 30°.[70] For $\theta_i = 0^o$, penetration increases from 56 to 73% with this increase in E_i and, for $\theta_i = 30^o$, penetration is less important and increases from 39 to 60%. Trapping was negligible for both θ_i. For Ar collisions with the C_{10} and C_{11} H-SAM and HO-SAM surfaces,[36] penetration of the surface increases with increase in E_i from 0.41 to 0.83 eV, i.e. the increase is from 5 to 19% for the C_{10} H-SAM and 7 to 15% for the C_{11} H-SAM. The amount of trapping is small 6% or less, but largest for the HO-SAM.

Collisions of $O(^3P)$ with the C_{12} H-SAM were studied for E_i of 0.10 to 5.22 eV and θ_i of 15° to 75°.[34] The percentage penetration increases with increase in E_i and decreases with increase in θ_i. For $\theta_i = 15^o$ and E_i of 0.10, 0.48, 3.25, and 5.22 eV the respective penetration percentages are 27, 53, 84, and 90%. The decrease in the penetration with increase in θ_i is illustrated by the E_i = 3.25 eV results, for which the penetration percentage is 84, 79, 59, 28, and 1 for θ_i of 15, 30, 45, 60 and 90 degrees, respectively.

Simulations of the dynamics for Xe-atom collisions with the {0001} surface of hexagonal ice[46,47] are also of interest. The percentage penetration is nearly independent of the collision energy ranging from 3.88 to 6.50 eV, but dependent on the incident angle. For E_i = 5.71 eV, the respective penetration percentage is 100, 100, 96, and 29 for θ_i of 0, 25, 45, and 65 degrees. Trapping which increases with increase in E_i, also decreases with increase in θ_i. For $\theta_i = 0^o$, the trapping percentage is 30, 48, 61, and 73 for the respective E_i of 3.88, 4.56, 5.71, and 6.50 eV. At E_i = 6.50 eV, the trapping percentage is 73, 57, 34, and 27 for θ_i of 0, 25, 45, and 65 respectively.

For the above simulations, the dynamics for Ne and O (^3P) colliding with a H-SAM and Ar colliding with a F-SAM are similar to those for ala_2-H^+ colliding with the F-SAM. For the ala_2-H^+ + F-SAM collisions, surface penetration becomes more important as the collision energy is increased, but trapping on/in the surface becomes less probable. The probabilities of both penetration and trapping decrease as the incident angle θ_i is increased. For the Ne, $O(^3P)$, and Ar collisions, penetration increases with increase in E_i, and decreases with increase in θ_i. However, the trapping dynamics are different for these three atoms as compared to ala_2-H^+. Trapping does not occur for Ne and is negligible for Ar. For the $O(^3P)$ collisions, trapping becomes more important with increase in E_i.

The dynamics for Xe + {0001} ice and CO_2 + C_8 F-SAM collisions are different than those for ala$_2$-H$^+$ + F-SAM. For Xe + ice, the surface penetration is nearly independent of the collision energy, while the trapping percentage increases with E_i. For the CO_2 + F-SAM collisions penetration decreases with increase in E_i.

V. Summary

Analyses were made of previous chemical dynamics simulations[41] of ala$_2$-H$^+$ + C_8 F-SAM collisions to determine the mechanistic details for collisional energy transfer and trapping/soft landing. The simulations were performed for collision energies E_i of 5-70 eV and incident angles θ_i of 0 and 45 degrees, with respect to the surface normal, for each E_i. There are four trajectory types: (1) direct scattering; (2) temporary sticking/physisorption on top of the surface; (3) temporary penetration of the surface with additional physisorption on the surface; and (4) trapping on/in the surface, by physisorption or surface penetration, when the trajectory is terminated. Trapping dominates at low E_i, as high as 84% for E_i = 5 eV and $\theta_i = 0^o$, while direct scattering dominates at high E_i, where all the scattering is direct at 70 eV. Temporary sticking/physisorption is as high as 18% for E_i = 5 eV and $\theta_i = 45^o$, while temporary penetration with additional physisorption is as high as 13% for E_i = 30 eV and $\theta_i = 0^o$. Somewhat surprisingly, energy transfers to ala$_2$-H$^+$ and the F-SAM are similar for trajectory types (1), (2), and (3). Energy transfer to ala$_2$-H$^+$ is primarily to vibration and not rotation. The largest transfer to rotation was found for E_i = 5 eV and $\theta_i = 45^o$, where the percentages to vibration and rotation are 87 and 13%, respectively.

As E_i is increased, trajectories penetrate the F-SAM more deeply. For the E_i = 70 eV and $\theta_i = 0^o$ simulations, all of the trajectories have at least one ala$_2$-H$^+$ heavy atom penetrating the F-SAM, and the average number of heavy atoms inside the F-SAM at the deepest penetration is 8.8. There are seven C-C midpoints for the $CF_3(CF_2)_7S$- chains of the F-SAM, and the deepest penetration is midpoint 2 and 5, respectively, for the 30 and 70 eV simulations with $\theta_i = 0^o$. For the low E_i of 5 and 13.5 eV only penetration of the top of the F-SAM is important and the average number ala$_2$-H$^+$ heavy atoms which penetrate the F-SAM is 0.7 for both of these E_i at $\theta_i = 0^o$. The average residence time for trajectories which temporarily physisorb and/or penetrate the F-SAM ranges from 1.0 to 3.6 ps, dependent on both E_i and θ_i .

It was found that adsorption and then trapping of ala_2-H^+ on the F-SAM is primarily a multi-step process, and the following adsorption/trapping mechanisms were identified for E_i of 5 and 13.5 eV with θ_i = 0°: (i) physisorption-penetration-physisorption (phys-pen-phys); (ii) penetration-physisorption-penetration (pen-phys-pen); (iii) penetration-physisorption (pen-phys); (iv) physisorption-penetration (phys-pen); and (v) only physisorption (phys). Given the statistical uncertainties, the pen-phys-pen, pen-phys, phys-pen, and phys trapping mechanisms have similar probabilities at 5 eV. For the 13.5 eV simulation, the phys-pen mechanism is unimportant. The dominant trapping mechanism at this energy is pen-phys, with 47% of the trajectories first penetrating and only 18% first physisorbing.

Direct comparisons with experiment are not possible for the ala_2-H^+ + F-SAM energy transfer and adsorption/trapping mechanisms found here. What may be compared with experiment is the percentage of the collision energy transferred to the ala_2-H^+ internal degrees of freedom. Experimentally the average of this percentage is independent of the collision energy in the range of 4.5 – 22.5 eV, for θ_i = 0°, and is 21%.[27] The simulations give 18 to 20 percent for the experimental collision energy range.[41]

The radius of gyration of the trapped ala_2-H^+ ions was calculated to investigate their conformational changes upon trapping. Trapping of ala_2-H^+ on/in the F-SAM decreases its compactness.

The penetration and trapping dynamics found in this study for ala_2-H^+ + F-SAM collisions were compared with those found in previous studies of projectile collisions with organic surfaces. Collisions of Ne, Ar, and $O(^3P)$ with SAM surfaces have similar penetration dynamics as found here for ala_2-H^+.

Acknowledgements

The research reported here is based upon work supported by the Robert A. Welch Foundation under grant No. D-0005 and the National Science Foundation under grant CHE-1416428. The authors also wish to thank the HPCC at Texas Tech University and Texas Advanced Computing Center (TACC) for the computational facilities they provided. Authors are particularly grateful for informative discussions with J. Laskin and S. A. Vázquez.

References

1. . J. C. Love; L. A. Estroff, J. K. Kriebel; R. G. Nuzzo, G. M. M. Whitesides, *Chem. Rev*. 2005, **105**, 1103
2. J. Laskin and J. H. Futrell, *J. Am. Soc. Mass Spectrom.* 2003, **14**, 1340-1347.
3. V. H. Wysocki, K. E. Joyce, C. M. Jones and R. L. Beardsley, *Am. Soc. Mass Spectrom.* 2008, **19**, 190-208.
4. V. Grill, J. Shen, C. Evans and R. G. Cooks, *Rev. Scientif. Instrum.* 2001, **72**, 3149-3179.
5. J. Alvarez, J. H. Furtell, and J. Laskin, *J. Phys. Chem. A* 2006, 110, 1678-1687.
6. J. Laskin, P. Wang and O. Hadjar, *Phys. Chem. Chem. Phys.* 2008, **10**, 1079-1090.
7. B. Gologan, J. R. Green, J. Alvarez, J. Laskin and R. G. Cooks, *Phys. Chem. Chem. Phys.* 2005, **7**, 1490-1500
8. P. Wang, O. Hadjar, P. L. Gassman and J. Laskin, *Phys. Chem. Chem. Phys.* 2008, **10**, 1512-1522.
9. V. H. Wysocki, C. M. Jones, A. S. Galhena and A. E. Blackwell, A. E. *J. Am. Soc. Mass Spectrom.* 2008, **19**, 903-913.
10. A. R. Dongre, A. Somogyi and V. H. Wysocki, *J. Mass Spectrom.* 1996, **31**, 339-350.
11. J. Laskin, Energy and Entropy Effects in Gas-Phase Dissociation of Peptides and Proteins. In *Principles of Mass Spectrometry Applied to Biomolecules*; Laskin, J, and Lifshitz, C., Eds.; John Wiley & Sons, Inc.: Hoboken, NJ, 2006.
12. S. A. Miller, H. Luo, S. J. Pachuta and R. G. Cooks, *Science* 1997, **275**, 1447-1450.
13. T. Pradeep, B. Feng, T. Ast, S. J. Patrick, R. G. Cooks and S. J. Pachuta, *J. Am. Soc. Mass Spectrom.* 1995, ***6,*** 187-194.
14. P. Wang, O. Hadjar and J. Laskin, *J. Am. Chem. Soc.* 2007, **129**, 8682-8683.
15. Q. Hu, P. Wang, P. L. Gassman and J. Laskin, *J. Anal. Chem.* 2009, **81**, 7302-7308.
16. W. A. Alexander, J. R. Morris and D. Troya, *J. Chem. Phys.* 2009, **130**, 084702
17. S. R. Cohen, R. Naaman and J. Sagiv, *Phys. Rev. Lett* 1987, **58**, 1208-1211; *Phys. Rev. Lett* 1987, **58**, 2153.
18. K. D. Gibson, N. Isa and S. J. Sibener, *J. Phys. Chem. A* 2006, **110**, 1469-1477.
19. S. F. Shuler, G. M. Davis, and J. R. Morris, *J. Chem. Phys*. 2002, **116**, 9147-9150
20. M. K. Ferguson, J. R. Lohr, B. S. Day and J. R. Morris, *Phys. Rev. Lett* 2004, **92**, 073201
21. J. Zhang, D. J. Garton and T. K. Minton, *J. Chem. Phys.* 2002, **117**, 6239-6251

22. M. E. Bennett, W. A. Alexander, J. W. Lu, D. Troya and J. R. Morris, *J. Phys. Chem. C* 2008, **112**, 17272-17280
23. Z. Ouyang, Z. Takáts, T. A. Blake, B. Gologan, A. J. Guyman, J. M. Wiseman, J. C. Oliver, V. J. Davisson and R. G. Cooks, *Science* 2003, **301**, 1351-1354
24. M. Volný, W. T. Elam, A. Branca, B. D. Ratner and F. Tureček, *Anal. Chem.* 2005, **77**, 4890-4896
25. M. Volný, A. Sengupta, C. B. Wilson, B. D. Swanson, E. J. Davis and F. Tureček, *Anal. Chem.* 2007, **79**, 4543-4551
26. J. Laskin, and J. Futrell, *J. Chem. Phys.* 2003, **119**, 3413-3420
27. J. Laskin, E. Denisov and J. Futrell, *J. Am. Chem. Soc.* 2000, **122**, 9703-9714
28. S. B. M. Bosio and W. L. Hase, *J. Chem. Phys.* 1997, **107**, 9677-9686
29. T. Y. Yan and W. L. Hase, *Phys. Chem. Chem. Phys.* 2000, **2**, 901-910
30. T. Y. Yan, N. Isa, K. D. Gibson, S. J. Sibener and W. L. Hase, *J. Phys. Chem. A* 2003, **107**, 10600-10607
31. T. Y. Yan and W. L. Hase, *J. Phys. Chem. B* 2002, **106**, 8029-8037
32. W. A. Alexander, J. Zhang, J. V. Murray, G. M. Nathanson and T. K. Minton, *Faraday Disc.* 2012, **157**, 355-374
33. D. Troya and G. C. Schatz, *J. Chem. Phys.* 2004, **120**, 7696-7707
34. U. S. Tasić, T. Y. Yan and W. L. Hase, *J. Phys. Chem. B* 2006, **110**, 11863-11877
35. E. Martĭnez-Núñez, A. Rahaman, and W. L. Hase, *J. Phys. Chem. C* 2007, **111**, 354-364
36. U. S. Tasić, B. S. Day, T. Y. Yan, J. R. Morris and W. L. Hase, *J. Phys. Chem. C* 2008, **112**, 476-490
37. O. Meroueh and W. L. Hase, *J. Am. Chem. Soc.* 2002, **124**, 1524-1531.
38. K. Park, B. Deb, K. Song and W. L. Hase, *Int. J. Mass Spectrom.* 2009, **20**, 939-948
39. G. L. Barnes and W. L. Hase, *J. Am. Chem. Soc.* 2009, **131**, 17185-17193
40. L. Yang, O. A. Mazyar, U. Lourderaj, J. Wang, M. T. Rodgers, E. Martĭnez-Núñez, S. V. Addepalli and W. L. Hase, *J. Phys. Chem. C* 2008, **112**, 9377-9386
41. S. Pratihar, S. C. Kohale, D. G. Bhakta, J. Laskin and W. L. Hase, *Phys. Chem. Chem. Phys.* 2014, **16**, 23769-23778
42. P. Wang and J. Laskin, *Angew. Chem. Int. Ed.* 2008, **47**, 6678-6680
43. R. G. Cooks, T. Ast, T. Pradeep and V. Wysocki, *Acc. Chem. Res.* 1994, **27**, 316-323.

44. J. Cyriac, T. Pradeep, K. Kang and R. Souda, R. G. Cooks, *Chem. Rev.* 2012, **112**, 5356-5411
45. O. Meroueh, Y. Wang and W. L. Hase, *J. Phys. Chem. A* 2002, **106**, 9983-9992
46. K. D. Gibson, D. R. Killelea, H. Yuan, J. S. Becker, S. Pratihar, P. Manikandan, S. C. Kohale, W. L. Hase and S. J. Sibener, *J. Phys. Chem. C* 2012, **116**, 1464-14273
47. S. Pratihar, S. C. Kohale, L. Yang, P. Manikandan, K. D. Gibson, D. R. Killelea, H. Yuan, S. J. Sibener and W. L. Hase, *J. Phys. Chem. C* 2013, **117**, 2183-2193
48. G. L. Barnes, K. Young, L. Yang and W. L. Hase, *J. Chem. Phys.* 2011, **134**, 094106
49. S. Pratihar, S. C. Kohale, S. A. Vázquez and W. L. Hase, *J. Phys. Chem. B* 2014, **118**, 5577-5588.
50. W. L. Hase, R. J. Duchovic, X. Hu, A. Kormonicki, K. Lim, D.-H. Lu, G. H. Peslherbe, N. K. Swamy, S. R. Vande Linde, A. J. C. Varandos, H. Wang and R. J. Wolfe, VENUS96. A General Chemical Dynamics Computer Program. *QCPE Bull*. 1996, **16**, 671.
51. X. Hu, W. L. Hase and T. Pirraglia, *J. Comput. Chem*. 1991, **12**, 1014-1024.
52. W. D. Cornell, P. Cieplak, C. I. Bayley, R. Gould, K. M. Merz, D. M. Ferguson, D. C. Spellmeyer, T. Fox, J. W. Caldwell and P. A. Kollman, *J. Am. Chem. Soc*. 1995, **117**, 5179-5197.
53. O. Borodin, G. D. Smith and D. Bedrov, *J. Phys. Chem. B* 2002, **106**, 9912-9922.
54. G.-Y. Liu, P. Fenter, C. E. D. Chidsey, D. F. Ogletree, P. Eisenberger, M. Salmeron, *J. Chem. Phys.* 1994, **110**, 4301-4306.
55. S. Chapman and D. L. Bunker, *J. Chem. Phys.* 1975, **62**, 2890-2899
56. W. L. Hase, D. M. Ludlow, R. J. Wolf and T. Schlick, *J. Phys. Chem.* 1981, **85**, 958-968.
57. G. H. Peslherbe, H. Wang and W. L. Hase, *Adv. Chem. Phys.* 1999, **105,** 171-201.
58. U. Lourderaj and W. L. Hase, *J. Phys. Chem. A* 2009, **113**, 2236-2253.
59. D. –h. Lu and W. L. Hase, *J. Phys. Chem.* 1988, **92**, 3217-3225.
60. D. –h Lu and W. L. Hase, *J. Phys. Chem* 1989, **91**, 7490-7497.
61. W. E. Milne, *Am. Math. Monthly.* 1926, **33**, 455.
62. D. L. Bunker, *Classical Trajectory Methods,* in *"Methods in Computational Physics"*, Academic Press, New York, 1971, **10**, 287-325.

63. A. Iserles, *A First Course in the Numerical Analysis of Differential equations*, Cambridge University Press, *1st Ed*., 1996.
64. B. S. Day, J. R. Morris, W. A. Alexander, and D. Troya, *J. Phys. Chem. A* 2006**, 110***,* 1319-1326.
65. W. A. Alexander, B. S. Day, H. J. Moore, T. R. Lee, J. R. Morris, and D. Troya, *J. Chem. Phys* 2008, **128**, 014713.
66. D. Troya, *Theor. Chem. Acc.* 2012, **113**, 1072.
67. T. Yan, W. L. Hase, and J. R. Barker, *Chem. Phys. Lett.*, 2000**, 329**, 84-91
68. T. Yan, W. L. Hase and J. C. Tully, *J. Chem. Phys.* 2004, **120**, 1031-1043
69. N. Isa, K. D. Gibson, T. Yan, W. L. Hase and S. J. Sibener, *J. Chem. Phys.* 2004, **120**, 2417-2433.
70. U. Tasić and D. Troya, *Phys. Chem. Chem. Phys*., 2008, **10**, 5776–5786

Table 1. Percentages of different ala_2-H^+ + F-SAM trajectory types

E_i (eV)	θ_i	Directly scatter[a]	Temporarily only physisorb[b]	Temporarily penetrate/physisorb[c]	Trapped[d]
5	0	12 ± 2	4 ± 1	0	84 ± 2
	45	13 ± 2	18 ± 2	0	69 ± 2
13.5	0	29 ± 2	4 ± 1	2 ± 1	65 ± 2
22.5	0	40 ± 2 (29)[e]	4 ± 1	15 ± 2	41 ± 2
	45	82 ± 2 (76)	6 ± 1	6 ± 1	6 ± 1
30	0	57 ± 3	1 ± 0.5	13 ± 2	29 ± 2
70	0	100	0	0	0

a. ala_2-H^+ directly scatters from F-SAM
b. ala_2-H^+ temporarily physisorbs on the F-SAM without penetration
c. ala_2-H^+ temporarily penetrates the F-SAM with physisorption
d. ala_2-H^+ is trapped on/in the F-SAM at the conclusion of the 10 ps trajectories.
e. Values in parentheses are percentages of direct scattering on top of the surface without any penetration from ref 41.

Table 2. Average residence times for temporarily physisorbed and/or penetrated trajectories[a]

E_i (eV)	θ_i	Temporarily only physisorb	Temporarily penetrate/physisorb
5	0	3.6	-
	45	3.2	-
13.5	0	2.5	3.0
22.5	0	2.2	1.1
	45	1.0	1.2
30	0	b	1.4
70	0	-	-

a. The average residence time τ_{res} is in units of ps.
b. There are too few trajectories of this type to determine a meaningful ensemble average.

Table 3. Average energy partitioning percentages for different trajectories.

E_i , θ_i	Type of trajectory[a]	$<\Delta E_{int}>$	$<\Delta E_{surf}>$	$<E_f>$	ΔE_{int} [b]	
					$<\Delta E_{vib}>$	$<\Delta E_{rot}>$
5 , 0°	Direct	20	72	8	92	8
	Physisorb	18	77	5	96	4
	Pen/Phys	-	-	-	-	-
5, 45°	Direct	23	59	18	87	13
	Physisorb	22	63	15	95	5
	Pen/Phys	-	-	-	-	-
13.5, 0°	Direct	19	76	5	91	9
	Physisorb	17	79	4	94	6
	Pen/Phys	15	83	2	95	5
22.5, 0°	Direct	21	74	5	92	8
	Physisorb	19	79	2	96	4
	Pen/Phys	18	80	2	97	3
22.5, 45°	Direct	17	60	17	86	14
	Physisorb	24	65	11	95	5
	Pen/Phys	24	66	10	96	4
30, 0°	Direct	19	77	4	93	7
	Physisorb	c	c	c	c	c
	Pen/Phys	17	81	2	97	3
70, 0°	Direct	17	81	2	96	4
	Physisorb	-	-	-	-	-
	Pen/Phys	-	-	-	-	-

a. The trajectory types are: direct scattering (Direct), physisorbed without penetration into the F-SAM (Physisorb), and penetration and physisorption (Pen/Phys).
b. The percentages for ΔE_{int} partitioning between ala_2-H^+ vibration and rotation.
c. There are too few trajectories of this type to determine meaningful ensemble average percentages.

Table 4. Mechanisms of trapping

E_i *(eV)*[a]	Phys-Pen-Phys	Pen-Phys-Pen	Pen-Phys	Phys-Pen	Phys
5	4 ± 1	21 ± 2	19 ± 2	15 ± 2	25 ± 2
13.5	2 ± 1	17 ± 2	30 ± 3	3 ± 1	13 ± 2

a. $\theta_i = 0^o$.

Table 5: Penetration and trapping for previous simulations of projectile + organic surface collisions [a]

E_i (eV)	θ_i	Properties	% Penetration	% Trapping	% $\langle E_f \rangle$	Trajectory Integration time (ps)	Ref.
			Ar + C_{12}, H-SAM				64
0.62, 0.83	30	5.4 [b]	23	26	6 (8)[c]	15	
		5.2		17	25		
		4.98		10	23		
		4.67		5	24		
		4.3		0.4	25		
			Ne, Ar, Kr, + C_{15}, H-SAM				65
0.62	30	Ne	15.0	1	21[d]	15	
		Ar	11.0	15	16		
		Kr	19.0	24	8		
			Ne, Ar, Kr, + C_{15}, F-SAM (semi fluorinated)				65
0.62	30	Ne	17.0	0	42[d]	15	
		Ar	4.0	7	25		
		Kr	6.0	19	8		
			Ne + C_6 H-SAM[e]				29
0.05	10		0	3	83 (-)[f]	3	
0.2			89	-	38 (60)		
0.4			96	-	23 (26)		
0.9			100	-	14 (12)		
0.05	30		0.1	-	-	3	
0.2			7	-	36 (50)		
0.4			16	-	24 (23)		
0.9			23	-	15 (11)		
0.05	45		-	-	-	3	
0.2			0.4	-	38 (64)		
0.4			4	-	26 (19)		
0.9			8	-	20 (9)		
			CO + C_{12}, H-SAM				16
0.62	30	0, 0[g]	~ 4%	30	13	15	
		0, 7		30	13		
		0, 14		41	13		
		0, 28		27	15		
		1, 0		30	13		
			CO + CF_3 terminated C_{12}-SAM				16
0.62	30	0, 0[g]	No	8	25[h]	15	
		0, 7	penetration	7	27		
		0, 14		6	28		
		0, 28		4	32		

		1, 0		6	26		
		OH radical + Perfluorinated C_8 -SAM					66
0.55	0	0, 1[i]	No	<1%	~35[j]	15	
		0, 3	penetration				
		0, 5					
		0, 7					
		CO_2 + C_8, F-SAM Surface					35
0.13	0		38	-	47 (40)[k]	150	
0.46	0		24	-	24 (11)		
0.87	0		25	-	20 (8)		

a. For penetration, the projectile penetrates the top-layer of the surface. Trapping represents trajectories which are on/in the surface when the trajectories are terminated. The surface is 300 K for all of the simulations.
b. Inter chain spacing in Å. Higher inter chain spacing indicates a lower density for the SAM surface.
c. For all direct scattered and trap-desorbed atoms at E_i = 0.83 eV. Values in parentheses are for E_i = 0.62 eV.
d. For all scattered atoms in single encounter collisions.
e. At $\theta_i = 60^o$ no penetration was observed.
f. Average final translational energy for all scattered Ne atoms. Values in parentheses are for trajectories that penetrate the SAM surface before scattering.
g. Vibrational and rotational quantum nos. of the projectile CO molecule.
h. Average translational energy of all CO molecules either directly scattered or trap-desorbed.
i. Vibrational and rotational quantum nos. of the OH radical.
j. Average final OH translational energy for all initial conditions of the OH radical.
k. Values in the parentheses are for trajectories which penetrate.

Figure Captions

Figure 1. Motion of the center-of-mass of ala_2-H^+ along the z-direction perpendicular to the Au-layer for three representative trajectories: (i) direct scattering; (ii) temporary penetration and physisorption followed by desorption; and (iii) trapping on/in the F-SAM surface at the conclusion of the trajectory. R on the y-axis indicates the distance of the ala_2-H^+ center-of-mass from the distance above/below the average 300 K position of the C-atoms of the -CF_3 groups. Simulations for E_i = 13.5 eV and $\theta_i = 0^o$.

Figure 2: Representative snapshots of deep penetration by two different 70 eV trajectories. ΔE_{int} versus τ_{res} Snapshots are taken by zooming into the surface, to achieve a clear view of depth of penetration along the z-direction. Only two CF_3-$(CF_2)_7$-S- chains are shown in the foreground. Color code: Au layer - orange spheres; S – yellow; C - cyan; N – blue; O – red; H - light grey; and F – purple.

Figure 3. Distributions of the deepest penetration of the F-SAM by an ala_2-H^+ heavy atom, for the E_i of 30 and 70 eV simulations with $\theta_i = 0^o$.

Figure 4. Scatter plot of for trajectories that directly scatter with one ITP, but also penetrate the surface for simulations of E_i = 30 eV and $\theta_i = 0^o$ collisions. ΔE_{int} are in kcal/mol.

Figure 5. Probability distribution of energy transfer to the ala_2-H^+ vibrational (red) and rotational (blue) degrees of freedom, for E_i = 13.5 eV and $\theta_i = 0^o$ collisions. Top panel is for all direct scattered trajectories and bottom panel is for temporarily physisorbed (with or without penetration) trajectories.

Figure 6. Probability distribution of energy transfer to the ala_2-H^+ vibrational (red) and rotational (blue) degrees of freedom, for E_i = 30 eV and $\theta_i = 0^o$ collisions. Top panel is for all direct scattered trajectories and bottom panel is for temporarily physisorbed (with or without penetration) trajectories.

Figure 7. Probability distribution of energy transfer to the ala_2-H^+ vibrational (red) and rotational (blue) degrees of freedom, for E_i = 70 eV and θ_i = 0° collisions. All the trajectories are direct scattered and they deeply penetrate the surface (see text).

Figure 8. Distribution of the average number of ala_2-H^+ heavy atoms which penetrate the F-SAM, f_{pen}, for the trajectories which are trapped on/in the F-SAM at the conclusion of the 10 ps trajectories. The value for f_{pen} is calculated as described in the text. Simulations for E_i of 5 and 13.5 eV, with $\theta_i = 0^o$.

Figure 9. Upper panel: Snapshots of ala_2-H^+ for two different R_g. Color code: C - cyan; N – blue; O – red; and H - light grey. Lower panel: Probability distributions of the radius of gyration (R_g) for trapped ala_2-H^+ at the termination of the 10 ps trajectories. Results for E_i of 5 and 13.5 eV, with $\theta_i = 0^o$.

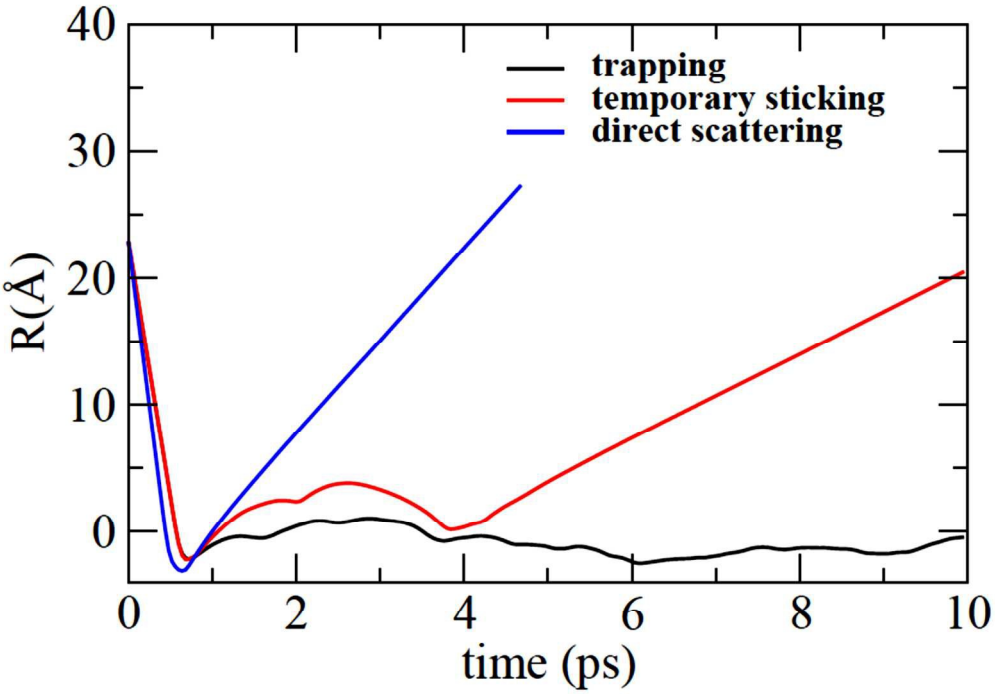

Figure 1.

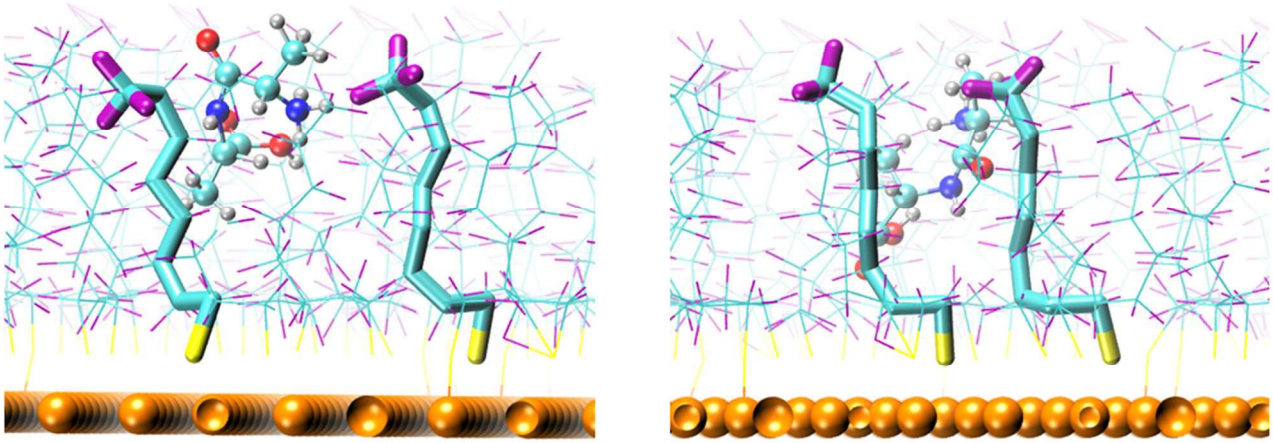

Figure 2.

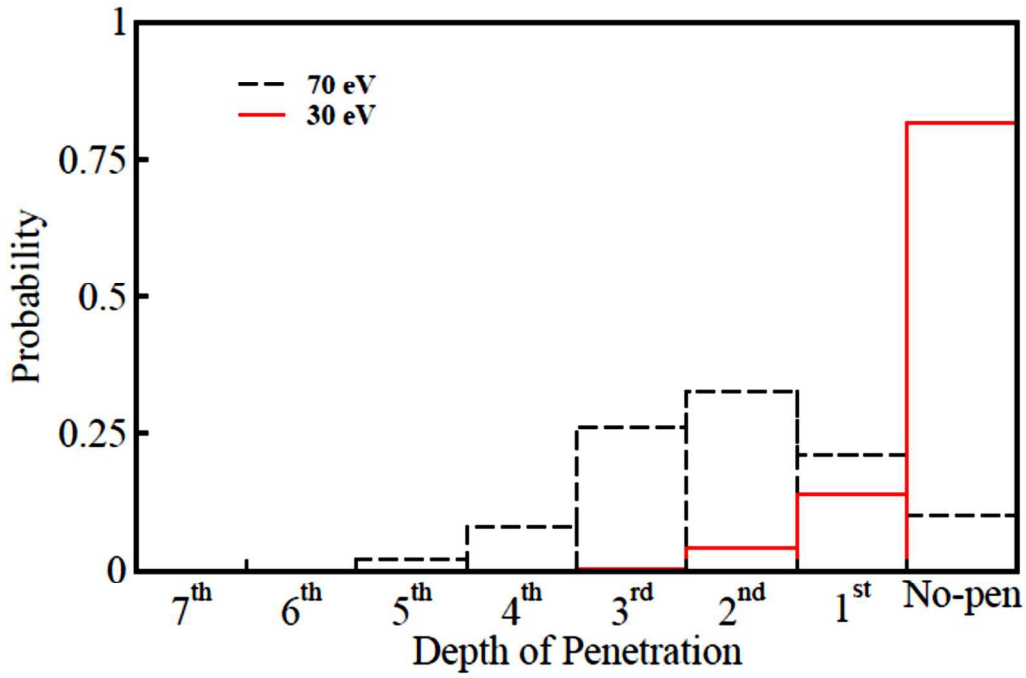

Figure 3.

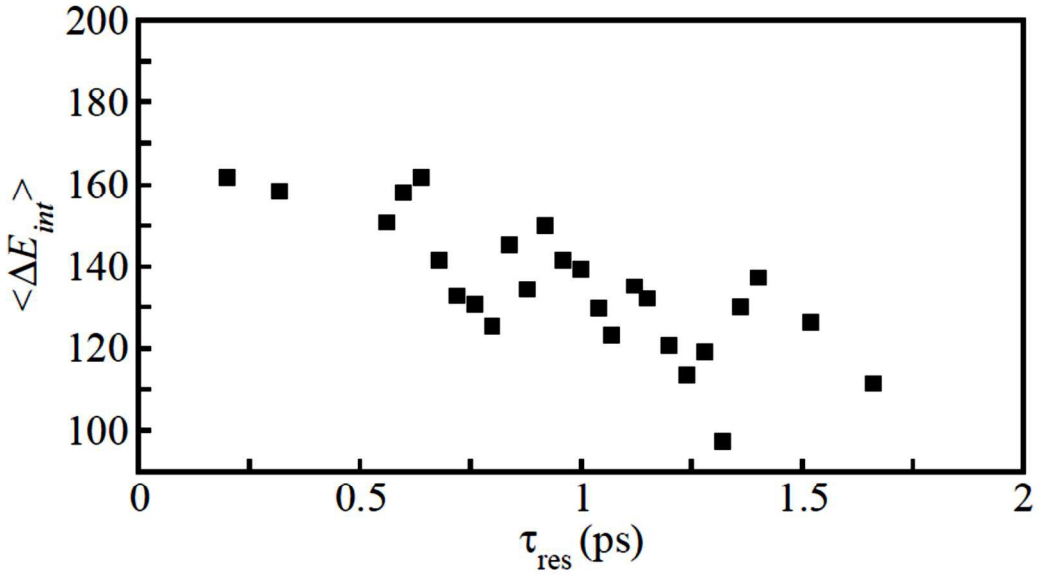

Figure 4.

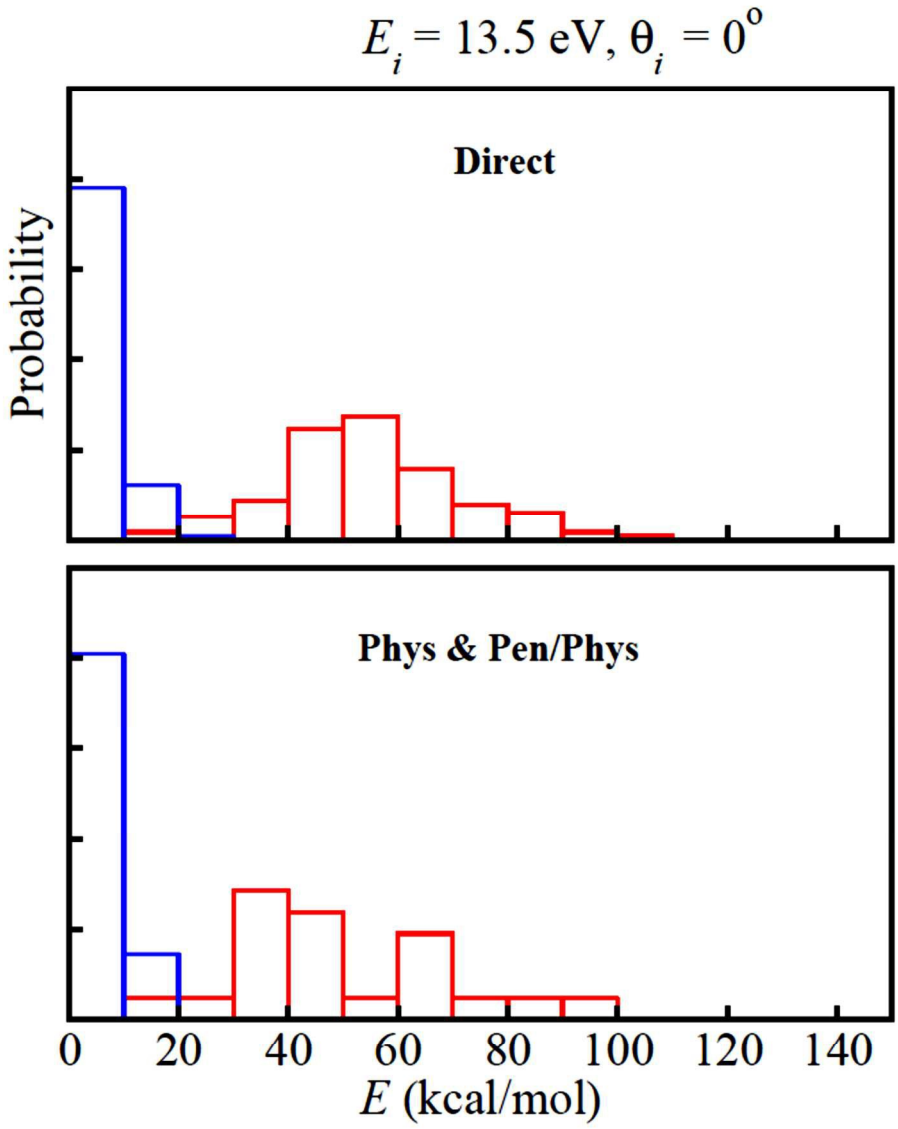

Figure 5.

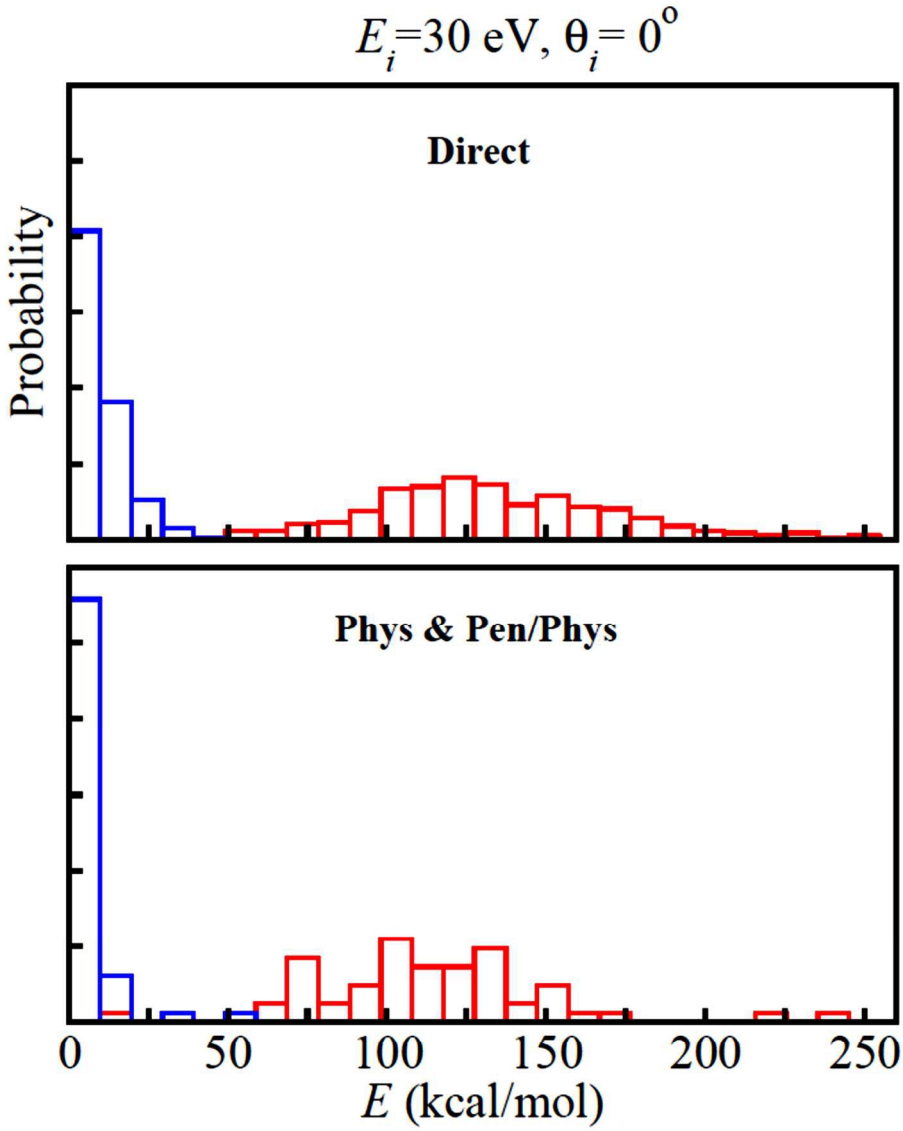

Figure 6.

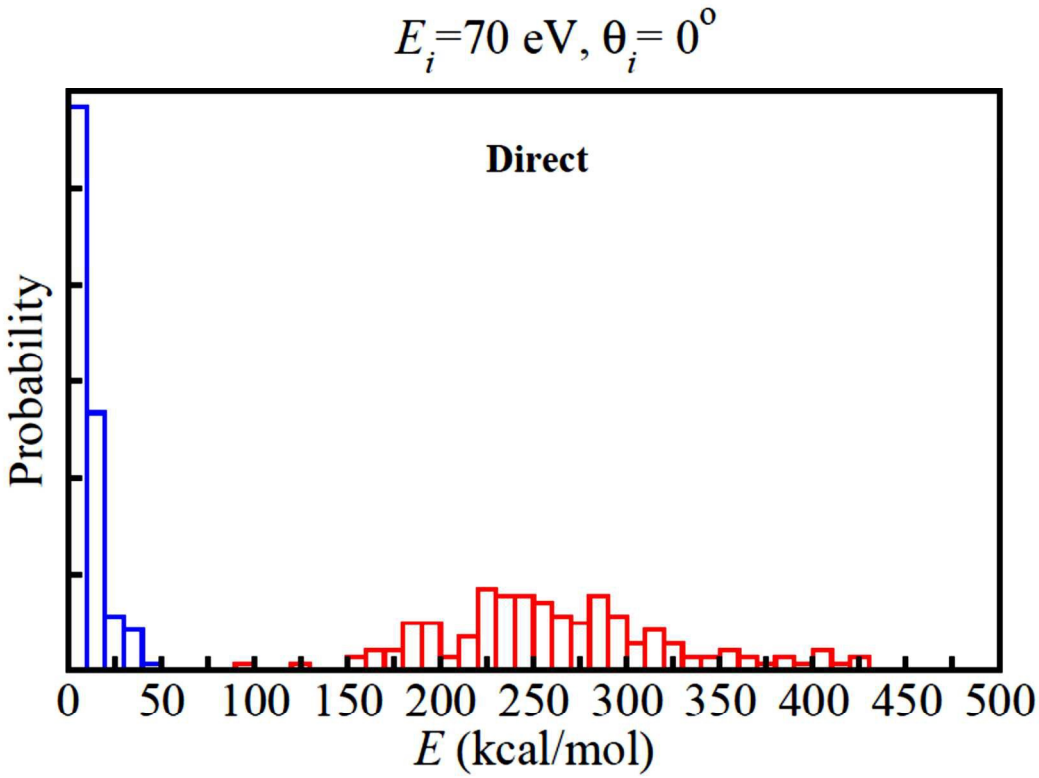

Figure 7.

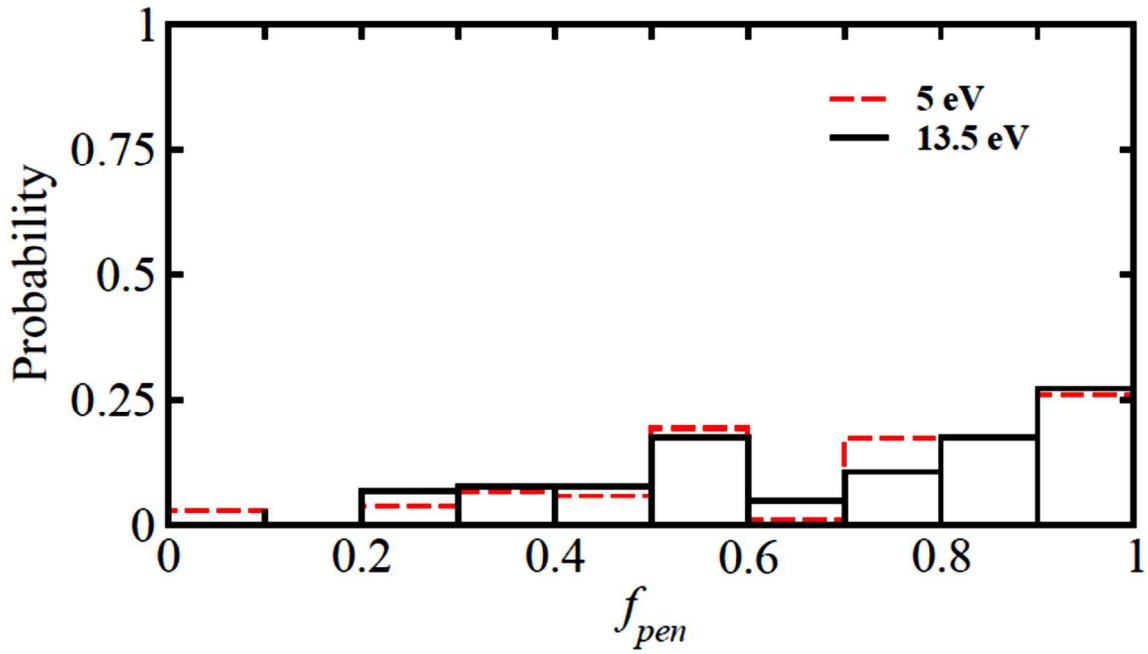

Figure 8.

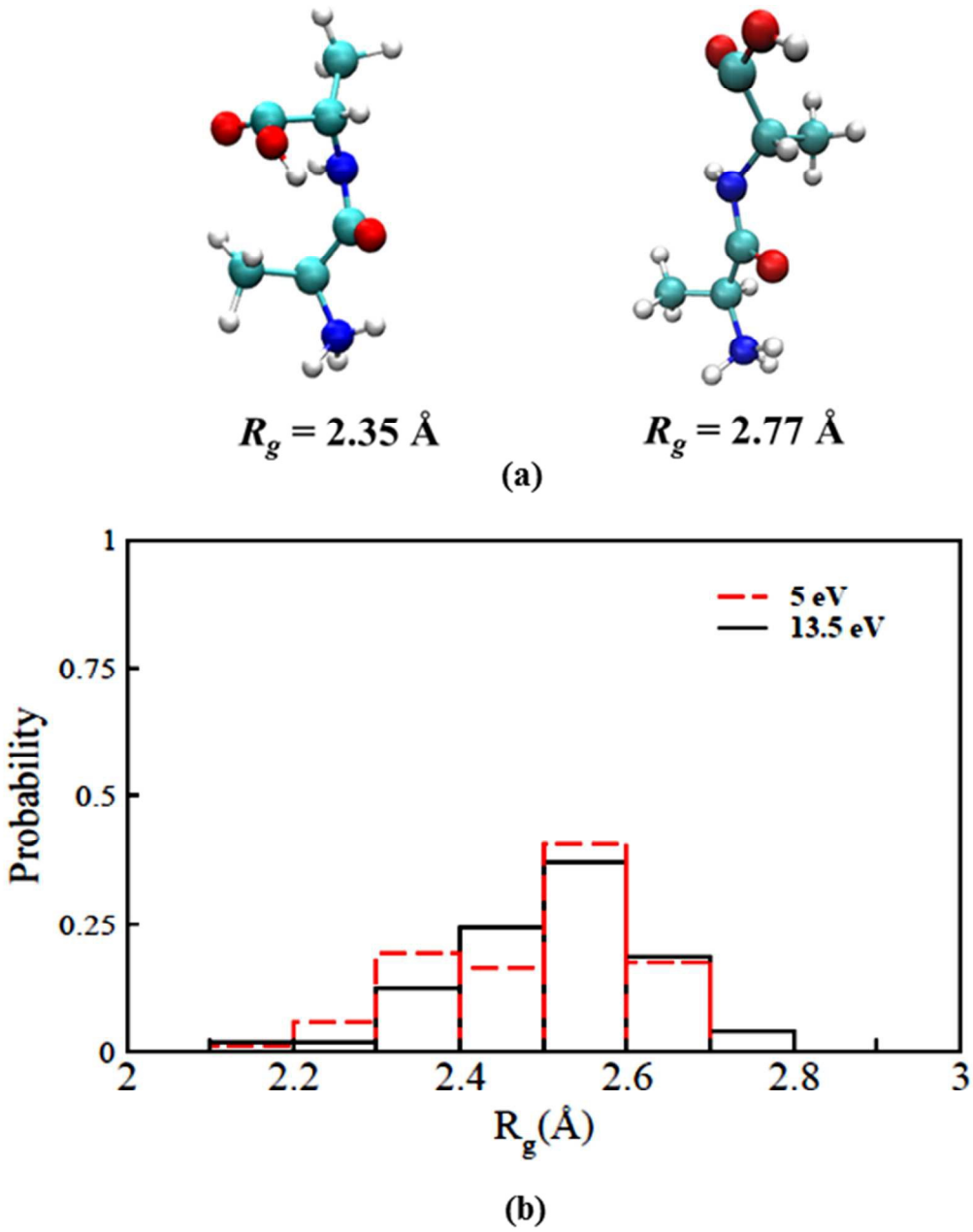

Figure 9.